nature materials

SUPPLEMENTARY INFORMATION

https://doi.org/10.1038/s41563-019-0465-6

In the format provided by the authors and unedited.

Critical role of intermediate electronic states for spin-flip processes in charge-transfer-type organic molecules with multiple donors and acceptors

Hiroki Noda[1,2,6], Xian-Kai Chen[3,6], Hajime Nakanotani[1,2,4*], Takuya Hosokai[2,5], Momoka Miyajima[1,2], Naoto Notsuka[1], Yuuki Kashima[1,2], Jean-Luc Brédas[3*] and Chihaya Adachi[1,2,4*]

[1]Center for Organic Photonics and Electronics Research, Kyushu University, Fukuoka, Japan. [2]JST, ERATO, Adachi Molecular Exciton Engineering Project, Kyushu University, Fukuoka, Japan. [3]School of Chemistry and Biochemistry, Center for Organic Photonics and Electronics, Georgia Institute of Technology, Atlanta, GA, USA. [4]International Institute for Carbon Neutral Energy Research, Kyushu University, Fukuoka, Japan. [5]National Metrology Institute of Japan, National Institute of Advanced Industrial Science and Technology, Tsukuba, Ibaraki, Japan. [6]These authors contributed equally: Hiroki Noda, Xian-Kai Chen. *e-mail: nakanotani@cstf.kyushu-u.ac.jp; jean-luc.bredas@chemistry.gatech.edu; adachi@opera.kyushu-u.ac.jp

SUPPLEMENTARY INFORMATION:

Title:

Critical role of intermediate electronic states for spin-flip processes in multi-donor-acceptor charge-transfer-type organic molecules

AUTHORs:

Hiroki Noda[1,2,#], Xian-Kai Chen[3,#], Hajime Nakanotani[1,2,4]*, Takuya Hosokai[2,5], Momoka Miyajima[1,2], Naoto Notsuka[1], Yuuki Kashima[1,2], Jean-Luc Brédas[3]* and Chihaya Adachi[1,2,4]*

AFFILIATIONs:

1. Center for Organic Photonics and Electronics Research (OPERA), Kyushu University, 744 Motooka, Nishi, Fukuoka 819-0395, Japan.

2. JST, ERATO, Adachi Molecular Exciton Engineering Project, c/o OPERA, Kyushu University, 744 Motooka, Nishi, Fukuoka 819-0395, Japan.

3. School of Chemistry and Biochemistry, Center for Organic Photonics and Electronics, Georgia Institute of Technology, Atlanta, Georgia 30332-0400, United States.

4. International Institute for Carbon Neutral Energy Research (WPI-I^2CNER), Kyushu University, 744 Motooka, Nishi, Fukuoka 819-0395, Japan.

5. National Metrology Institute of Japan, National Institute of Advanced Industrial Science and Technology (AIST), Tsukuba Central 2, 1-1-1 Umezono, Tsukuba, Ibaraki 305-8568, Japan.

# These authors contributed equally to this work.

CONTENTS

Supplementary Methods:

Materials

4CzIPN, *m*-2CzIPN, 5CzBN, *o*-3CzBN, *m*-3CzBN and o-2DPABMe were synthesized according to literature.[1-4)]

1) 1,5-dibromo-2,3,4-tri(9H-carbazol-9-yl)benzene (*o*-3Cz2Br)

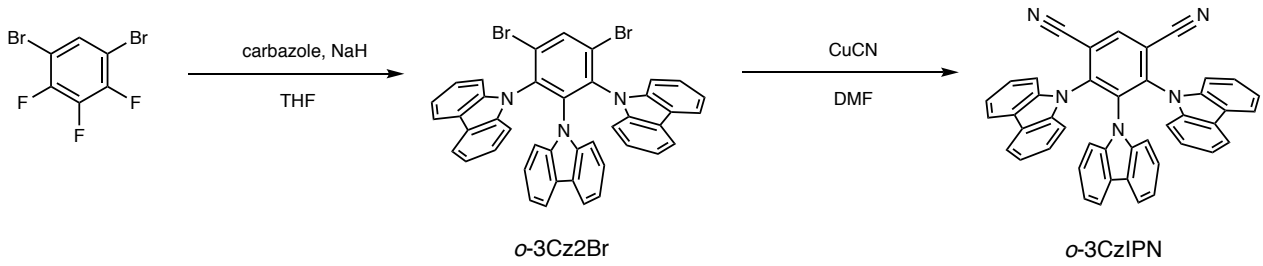

o-3Cz2Br *o*-3CzIPN

First, carbazole (2.3 g, 13.8 mmol) was added to a dispersion of sodium hydride (60% in mineral oil 0.55 g, 13.8 mmol) in anhydrous THF (40 ml) at 0 °C. After stirring for 30 min, 1,5-dibromo-2,3,4-trifluorobenzene (1.0 g, 3.45 mmol) was added to the mixed solution under argon atmosphere. The reaction mixture was stirred at room temperature overnight. The reaction mixture was quenched with water and the precipitate was filtered and washed with water and methanol. The obtained solid was further washed by acetone. Then we used *o*-3Cz2Br without further purification.

2) 4,5,6-tri(9H-carbazol-9-yl)isophthalonitrile (*o*-3CzIPN)

To a solution of o-3Cz2Br (0.8 g) in DMF (10 ml) was added copper (I) cyanide (0.21g, 2.4 mmol). The solution was refluxed overnight. The reaction mixture was cooled to room temperature and poured into a 10% solution of NaOH. The organic layer was extracted using dicloromethane and washed with water, brine and dried over anhydrous Na_2SO_4, filtered and concentrated in *vacuo*. The crude product was purified by column chromatography on silica gel (toluene) and then reprecipitated from toluene and methanol to produce *o*-3CzIPN as yellow powder (total; 0.41 g 0.66 mmol, 19%).

^{1}H NMR: (500 MHz, acetone-d_6): δ (ppm) = 9.15 (s, 1H), 7.82 (m, 4H), 7.50 (m, 4H), 7.37 (d, J = 7.5 Hz, 2H), 7.29 (d, J = 8.2 Hz, 2H), 7.08 (m, 8H), 6.76 (t, J = 7.9 Hz, 2H), 7.44 (t, J = 8.4 Hz, 2H)

^{13}C NMR: (125 MHz, $CDCl_3$): δ (ppm) = 144.14, 138.28, 137.56, 137.02, 125.62, 124.62, 124.35, 123.72, 121.70, 120.77, 120.29, 119.50, 115.31, 114.09, 110.04, 109.38

MS (FD-MS): m/z 625.13 $[M+H]^+$, (623.21 calcd for $C_{44}H_{25}N_5$)

Elemental analysis: calcd. for $C_{44}H_{25}N_5$: C, 84.73; H, 4.04; N, 11.23; found: C, 84.69; H, 3.99; N, 11.29.

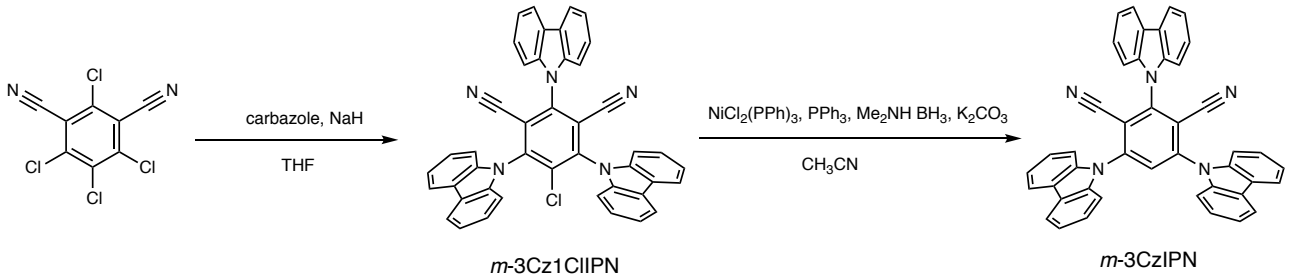

3) 3-chloro-2,4,6-tri(9H-carbazol-9-yl)isophthalonitrile (*m*-3Cz1ClIPN)

First, carbazole (2.8 g, 16.9 mmol) was added to a dispersion of sodium hydride (60% in mineral oil 0.68 g, 16.9 mmol) in anhydrous THF (60 ml) at 0 °C. After stirring for 30 min, tetrachloroisophthalonitrile (1.5 g, 5.64 mmol) was added to the mixed solution under argon atmosphere. The reaction mixture was stirred at room temperature overnight. The reaction mixture was quenched with water and the precipitate was filtered and washed with water and methanol. The obtained solid was purified by column chromatography on silica gel (toluene) and then reprecipitated from toluene/methanol to produce *m*-3Cz1ClIPN as yellow powder (2.75 g, 4.18 mmol, 74%).

^{1}H NMR: (500 MHz, acetone-d_6): δ (ppm) = 8.29 (m, 6H), 7.78 (d, J = 8.2 Hz, 2H), 7.68 (d, J = 8.3 Hz, 4H), 7.57 (m, 6H), 7.42 (m, 6H)

^{13}C NMR: (125 MHz, $CDCl_3$): δ (ppm) = 145.07, 144.23, 139.72, 139.23, 137.04, 126.93, 126.90, 124.79, 124.61, 122.44, 122.18, 121.32, 121.23, 117.62, 110.69, 109.48, 109.29

MS (FD-MS): m/z 658.12 $[M+H]^+$, (657.17 calcd for $C_{44}H_{24}ClN_5$)

4) 2,4,6-tri(9H-carbazol-9-yl)isophthalonitrile (*m*-3CzIPN)

A mixture of *m*-3Cz1ClIPN (0.5 g, 0.76 mmol), bis(triphenylphosphine)nickel(II) dichloride (14.9 mg, 0.023 mmol), triphenylphosphine (5.98 mg, 0.023 mmol), 98% borane– dimethylamine

complex (50 mg, 0.84 mmol) and potassium carbonate (0.12 g, 0.84 mmol) in 5 ml of acetonitrile was heated and stirred at 40 °C overnight. After cooling, the mixture was filtered through Celite. The organic layer was separated, and the aqueous layer was extracted with the chloroform. The mixture was concentrated in *vacuo*. The crude product was purified by column chromatography on silica gel (toluene:hexane, 4:1 v/v) to give *m*-3CzIPN (190 mg, 0.30 mmol, 40%).

^{1}H NMR: (500 MHz, acetone-d_6): δ (ppm) = 8.69 (s, 1H), 8.31 (d, J = 7.8 Hz, 4H), 8.25 (d, J = 7.7 Hz, 4H), 7.82 (m, 6H), 7.61 (t, J = 8.3 Hz, 2H), 7.55 (t, J = 8.4 Hz, 4H), 7.42 (m, 6H)

^{13}C NMR: (125 MHz, $CDCl_3$): δ (ppm) = 148.12, 147.10, 140.06, 139.52, 128.02, 126.92, 126.88, 124.93, 124.81, 122.50, 122.21, 121.32, 121.09, 112.43, 111.71, 109.87, 109.35

MS (MALDI-TOF MS): m/z 624.14 $[M+H]^+$, (623.21 calcd for $C_{44}H_{25}N_5$)

Elemental analysis: calcd. for $C_{44}H_{25}N_5$: C, 84.73; H, 4.04; N, 11.23; found: C, 84.69; H, 4.00; N, 11.28.

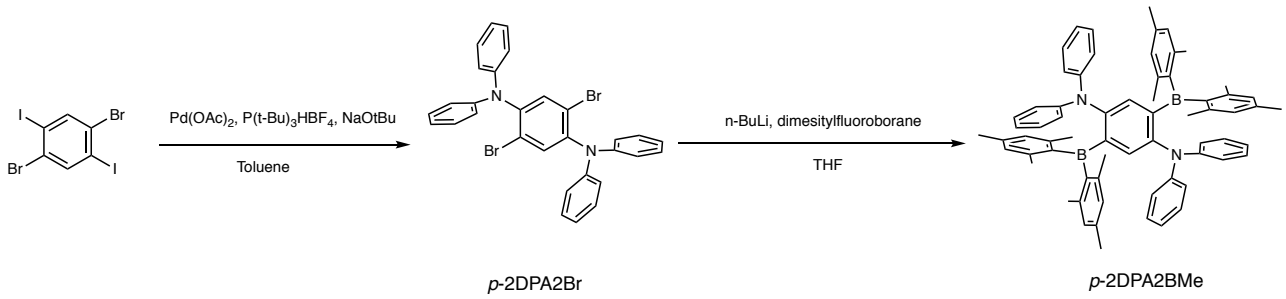

p-2DPA2Br　　*p*-2DPA2BMe

5) 2,5-dibromo-N^1,N^1,N^4,N^4-tetraphenyl-1,4-benzenediamine (*p*-2DPA2Br)

A mixture of 1,4-dibromo-2,5-diiodobenzene (3.0 g, 6.15 mmol), diphenylamine (2.1 g, 12.3 mmol), palladium(II) acetate (0.14 g, 0.615 mmol), tri-tert-butylphosphonium tetrafluoroborate (0.36 g, 1.23 mmol) and sodium tert-butoxide (2.36 g, 24.6 mmol) in 60 ml of toluene was heated and stirred at 100 °C overnight. After cooling, the mixture was filtered through Celite. The organic layer was separated, and the aqueous layer was extracted with the dichloromethane. The mixture was concentrated in *vacuo*. The crude product was purified by column chromatography on silica gel (dichloromethane:hexane, 1:6 v/v) to give *p*-2DPA2Br (1.03 g, 1.81 mmol, 29%).

^{1}H NMR: (500 MHz, acetone-d_6): δ (ppm) = 7.56 (s, 2H), 7.31 (t, J = 8.0 Hz, 8H), 7.03 (m, 12H)

^{13}C NMR: (125 MHz, $CDCl_3$): δ (ppm) = 146.64, 143.96, 135.99, 129.27, 122.68, 122.60, 122.38

MS (FD-MS): m/z 571.07 $[M+H]^+$, (570.33 calcd for $C_{30}H_{22}Br_2N_2$)

6) 2,5-bis(dimesitylboranyl)- *N*^{1},*N*^{1},*N*^{4},*N*^{4}-tetraphenyl-1,4-benzenediamine (*p*-2DPA2BMe)

To a solution of p-2DPABr (0.50 g, 0.88 mmol) in THF at −78 °C was added dropwise n-BuLi in hexane (1.6 M, 1.21 ml, 1.94 mmol). The mixture was stirred for 30 min at -78 °C. Dimesitylboron fluoride (0.52 g, 1.94 mmol) was added to this solution and stirred at 0 °C overnight. After reaction, water was added to the solution and the organic layer was extracted by dichloromethane. The mixture was concentrated in *vacuo*. The crude product was purified by column chromatography on silica gel (dichloromethane:hexane, 1:5 v/v) to give *p*-2DPA2BMe (0.07 g, 0.07 mmol, 8.8%).

^{1}H NMR: (500 MHz, $CDCl_3$): δ (ppm) = 6.99 (m, 10H), 6.81 (t, *J* = 7.3 Hz, 4H), 6.55 (d, *J* = 7.6 Hz, 8H), 6.52 (s, 8H), 2.14 (s, 12H), 1.74 (s, 24H)

^{13}C NMR: (125 MHz, $CDCl_3$): δ (ppm) = 149.43, 149.24, 142.46, 140.41, 138.24, 137.95, 128.33, 128.05, 124.40, 121.90, 23.43, 21.11

MS (FD-MS): m/z 909.70 $[M+H]^+$, (908.89 calcd for $C_{66}H_{66}B_2N_2$)

Elemental analysis: calcd. for $C_{66}H_{66}B_2N_2$: C, 87.22; H, 7.32; N, 3.08; found: C, 87.51; H, 7.28; N, 3.11.

Supplementary Information:

Modulation of intersystem crossing rate by solvation

Because organic molecules exhibiting TADF commonly contain strong electron-donor and electron-acceptor moieties to achieve a small ΔE_{ST}, the molecules should naturally form CT-type excited states for both singlets and triplets. Hence, although k_{ISC} and k_{RISC} are critical parameters to evaluate TADF properties in organic molecules exhibiting TADF, k_{ISC} and k_{RISC} can be greatly affected by the polarity of the surrounding matrix, whether a solvent or solid-state host. In this section, we show the effect of the matrix polarity on the forward ISC process and reveal that the E_A^{ISC} in 5CzBN appears when the $^1CT_1$ is stabilized by the solvation.

The $^1CT_1$ energy of 5CzBN is estimated to be 2.94 eV in toluene and 2.80 eV in CH_2Cl_2 (**Fig. S7a**). Furthermore, the $^1CT_1$ energy of 5CzBN can be precisely modulated by systematically changing the environment polarity using a mixture of toluene and CH_2Cl_2, confirming the stabilization of $^1CT_1$ by solvation. In contrast to the case of 5CzBN, the S_1 energy of 4CzBN hardly changes even with increasing polarity (**Figure S8**; the $^1CT_1$ stabilized from 3.01 eV for toluene to 2.96 eV for CH_2Cl_2), indicating that the solvation effect on the excited states is weaker for 4CzBN than 5CzBN. Therefore, changes of energy level positions among S_1, T_n, and T_1 depend on the environment polarity for 5CzBN.

Figure S7b shows the transient PL decay profiles of 5CzBN in different solvents on a nanoseconds time scale. The prompt fluorescence lifetime (τ_P) of 5CzBN increases with increasing polarity (from 3.7 ns in toluene to 12.0 ns in CH_2Cl_2). In addition, a high total PLQY of over 70% was confirmed in all samples as summarized in **Table S1**, indicating no significant difference in the total PLQY with a change of the environment polarity (ε =2.4–3.1) in the case of 5CzBN.

Importantly, we confirmed no significant decrease of the radiative decay rate constant from singlet state (k_r^S) in 5CzBN because the PLQY component from prompt fluorescence (Φ_{PL_PF}) simultaneously increases with increasing polarity (Φ_{PL_PF} = 7% in toluene and Φ_{PL_PF} = 16% in CH_2Cl_2).

Therefore, the increase of τ_P should related to a limiting of the forward ISC process. Indeed, the k_{ISC} of 5CzBN in CH_2Cl_2 is calculated to be 7.0×10^7 s^{-1}, and this value is less than one-third of that in toluene ($k_{ISC} = 2.5 \times 10^8$ s^{-1}), indicating the restriction of forward ISC in 5CzBN in a highly polar environment. The dependence of k_{ISC} on the environment polarity is further confirmed even in a mixed solvent (toluene:CH_2Cl_2), as summarized in **Table S1**. Although k_{RISC} also changed with polarity, the variation of k_{RISC} is only 1.3 times, indicating that the polarity change mainly affects the forward ISC process in 5CzBN.

Table S1: Photophysical properties of 5CzBN in various solvent.

Solvent	Φ_{PL} (%)[*1]	τ_p (ns)	τ_d (μs)	k_r (10^7 s^{-1})	k_{ISC} (10^8 s^{-1})	k_{RISC} (10^5 s^{-1})	E_A^{ISC} (meV)	E_A^{RISC} (eV)	S_1 (eV)
toluene	7 / 74	3.7	47	1.9	2.5	2.2	N.A.	0.12	2.94
1:1[*2]	13 / 80	8.2	23	1.6	1.0	2.6	36	0.11	2.84
dichloromethane	16 / 73	12	15	1.3	0.7	2.9	45	0.13	2.80

[*1] PLQY of 5CzBN before / after Ar bubbling.
[*2] The ratio of toluene: dichloromethane mixed solvent.

To evaluate the origin of the restriction of the forward ISC process, the temperature dependence of k_{ISC} was measured in solution samples. **Figure S7c** shows the Arrhenius plots for k_{ISC} of 5CzBN in toluene, mixed (1:1) solvent, and CH_2Cl_2. Although no temperature dependence of k_{ISC} in toluene solution was observed, a decrease of k_{ISC} with temperature was confirmed in the mixed (1:1) solvent and CH_2Cl_2. Using the Arrhenius equation, the E_A^{ISC} for 5CzBN was calculated to be 37 meV in the mixed (1:1) solvent and 45 meV in CH_2Cl_2. The observation of E_A^{ISC} in the mixed (1:1) and CH_2Cl_2 solutions indicates that the forward ISC process in 5CzBN becomes an uphill process when the $^1CT_1$ is stabilized from 2.94 eV to 2.80 eV. Importantly, there is the large difference between E_A^{RISC} (130 meV) and E_A^{ISC} (45 meV) in CH_2Cl_2 solution, corroborating that the spin-flip processes proceeds through a specific intermediate excited state.

Supplementary Figure: Fig. S1

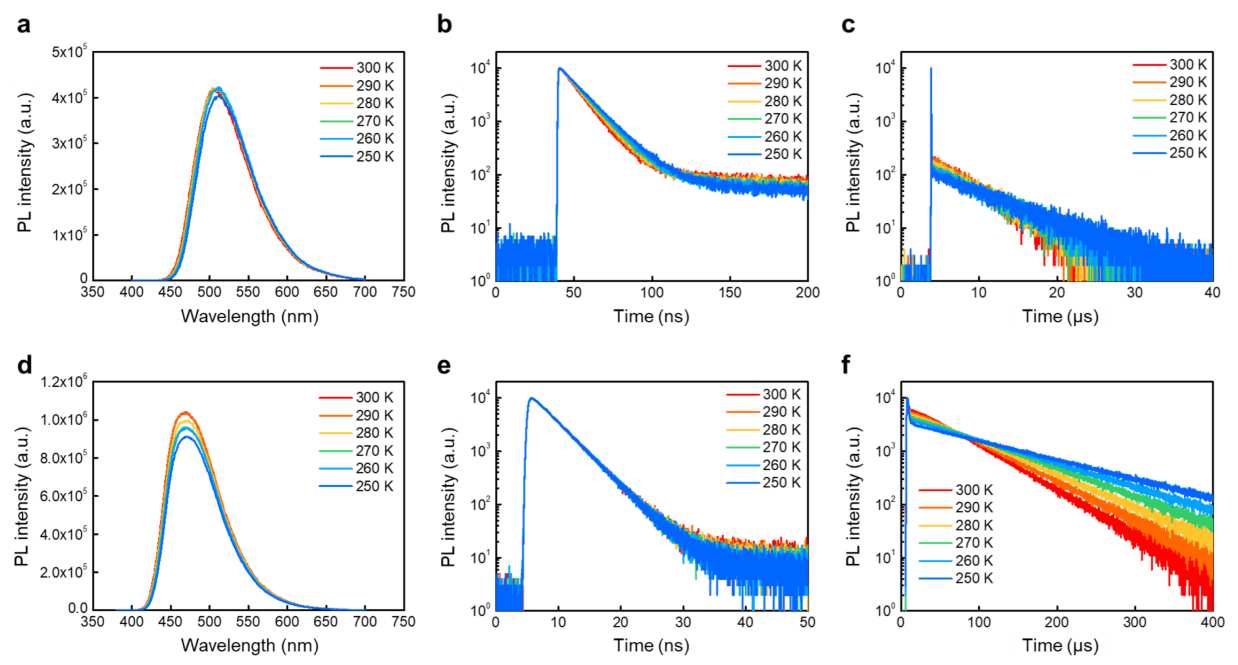

Supplementary Figure 1 | PL spectrum and transient PL decay profile of CzCN derivatives in solution. PL spectrum, nano-seconds and micro-seconds PL decay profile of 4CzIPN (a, b, c) and 5CzBN (d, e, f) in toluene solutions at different temperature.

Supplementary Figure: Fig. S2

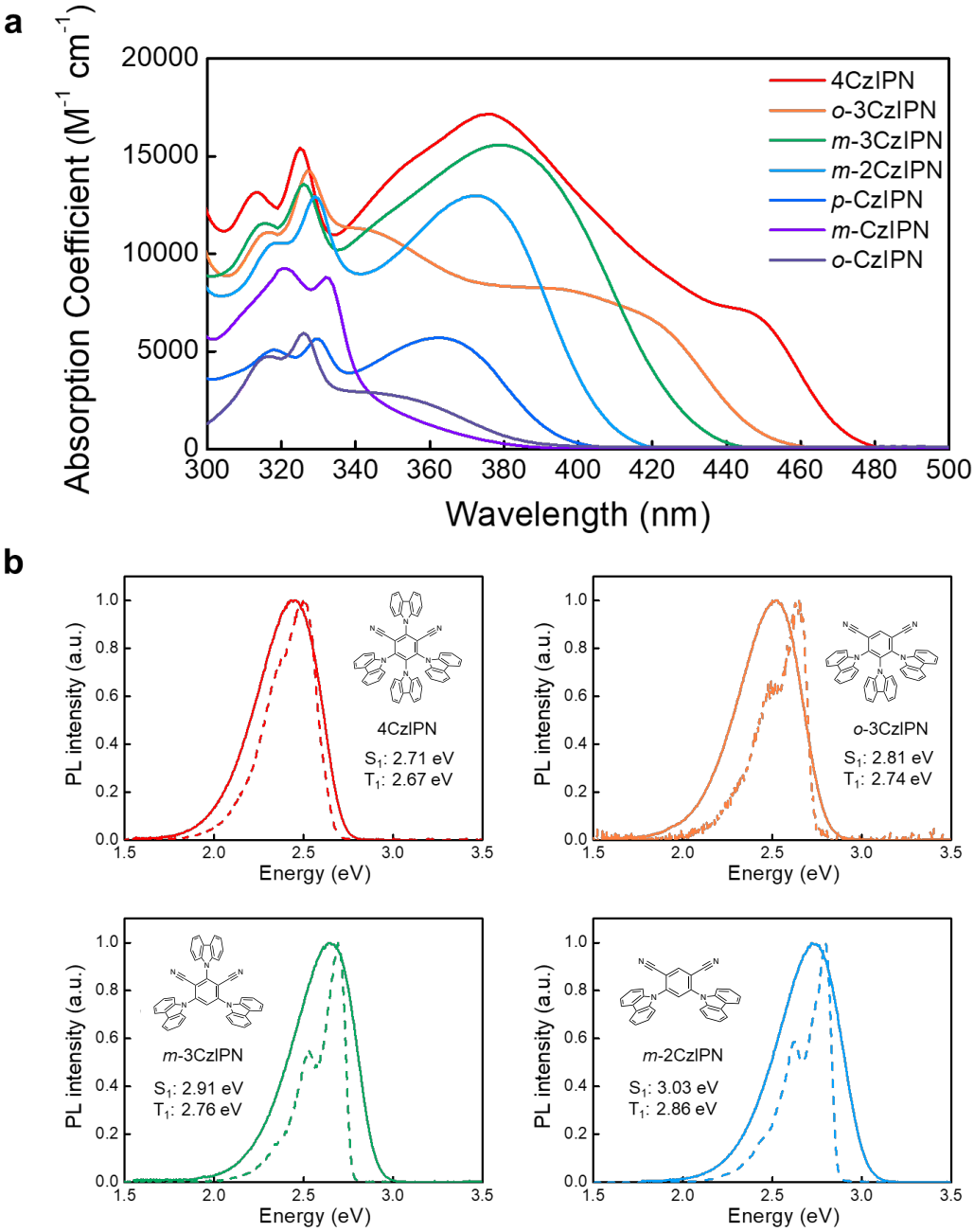

Supplementary Figure 2 | Photoluminescence characteristics of CzCN derivatives in solution. (a) Absorption coefficient spectra of 4CzIPN, *o*-3CzIPN, *m*-3CzIPN, *m*-2CzIPN, *p*-CzIPN, *m*-CzIPN, and *o*-CzIPN in toluene at a concentration of 10^{-5} mol L^{-1}. (b) Fluorescence spectra (solid line) and phosphorescence spectra (dashed line) of 4CzIPN, *o*-3CzIPN, *m*-3CzIPN, and *m*-2CzIPN in 10^{-5} mol L^{-1} toluene solutions. Phosphorescence spectra were measured in 10^{-5} mol L^{-1} toluene solutions at 77 K.

Supplementary Figure: Fig. S3

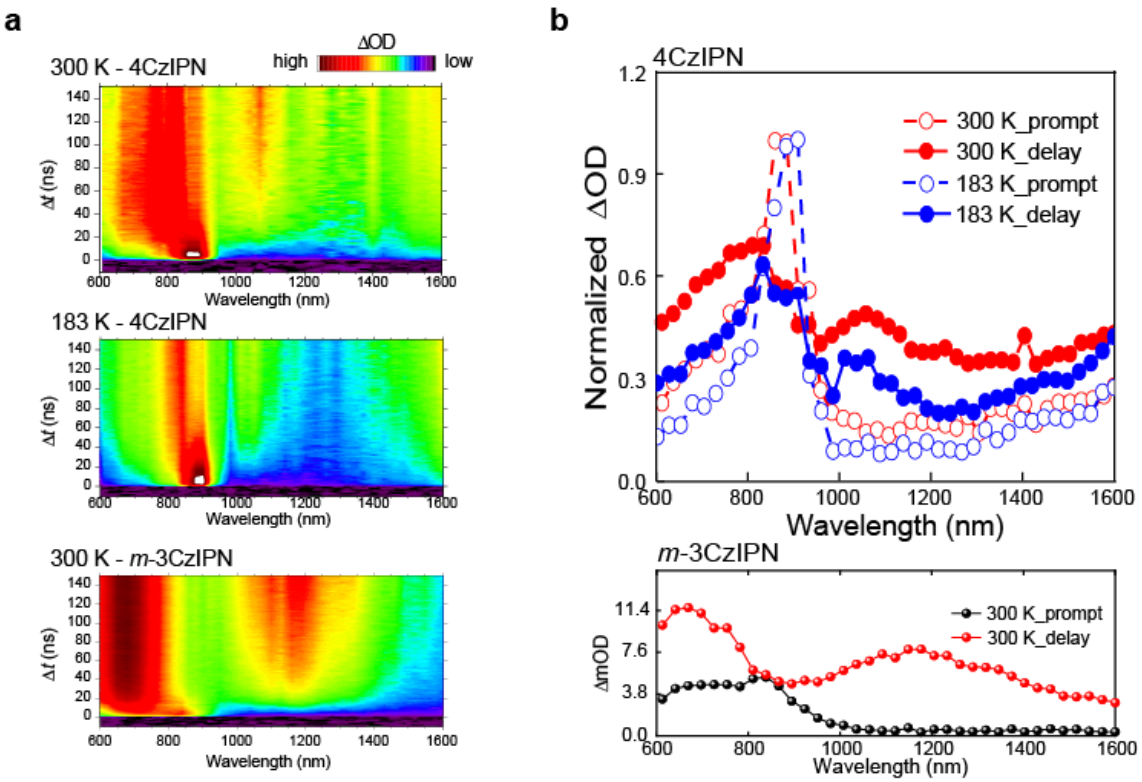

Supplementary Figure 3 | Temperature dependence of TAS contour map of CzCN derivatives in solution. (a) Contour maps of transient absorption spectra of 4CzIPN and *m*-3CzIPN in toluene at a concentration of 10^{-4} mol L^{-1} at 300 K and/or 183 K. (b) The TAS spectra of the prompt (Δt = 4.5 to 5.5 ns) and delay (Δt = 50 to 100 ns) states of 4CzIPN at 300 K and 183 K, where the spectra of *m*-3CzIPN at 300 K is also compared.

Supplementary Figure: Fig. S4

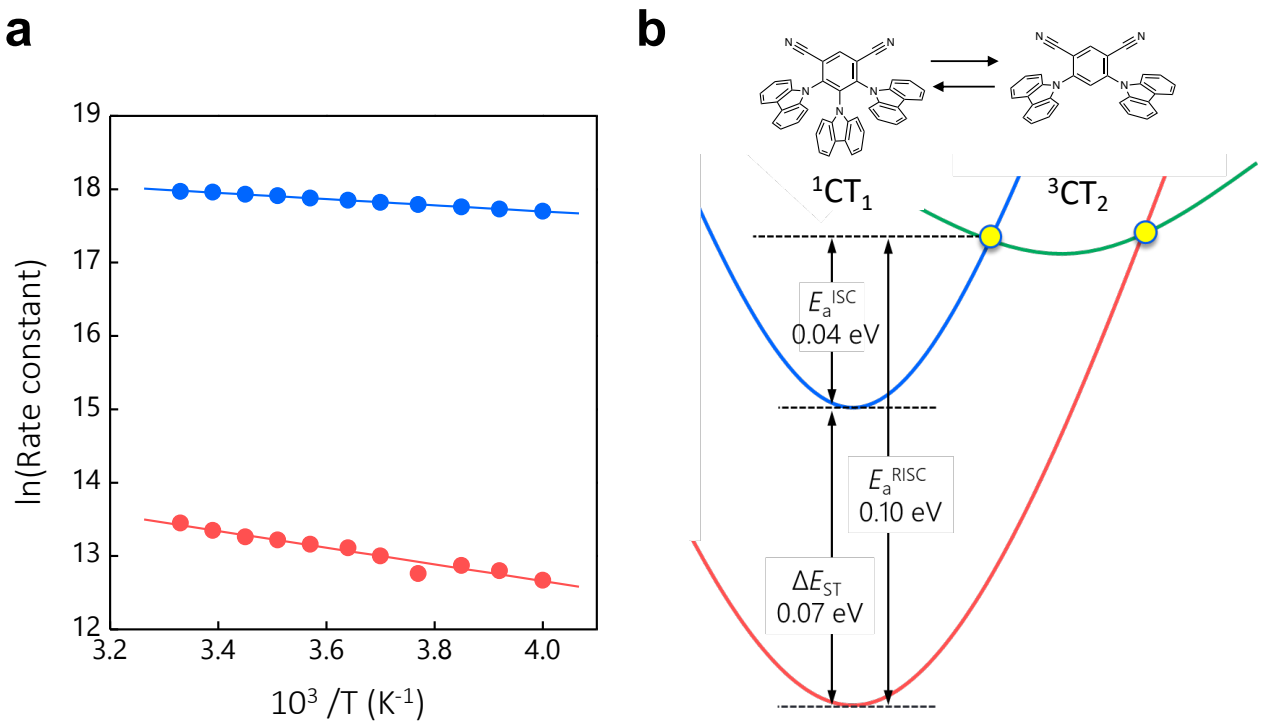

Supplementary Figure 4 | Spin-flip process through an intermediate higher-lying triplet excited state of *o*-3CzIPN. (a) Arrhenius plot of forward ISC (blue circle) and reverse ISC (red circle). The activation energies of forward and reverse ISC are 0.04 eV and 0.10 eV respectively. (b) The proposed energy potential surfaces for *o*-3CzIPN.

Supplementary Figure: Fig. S5

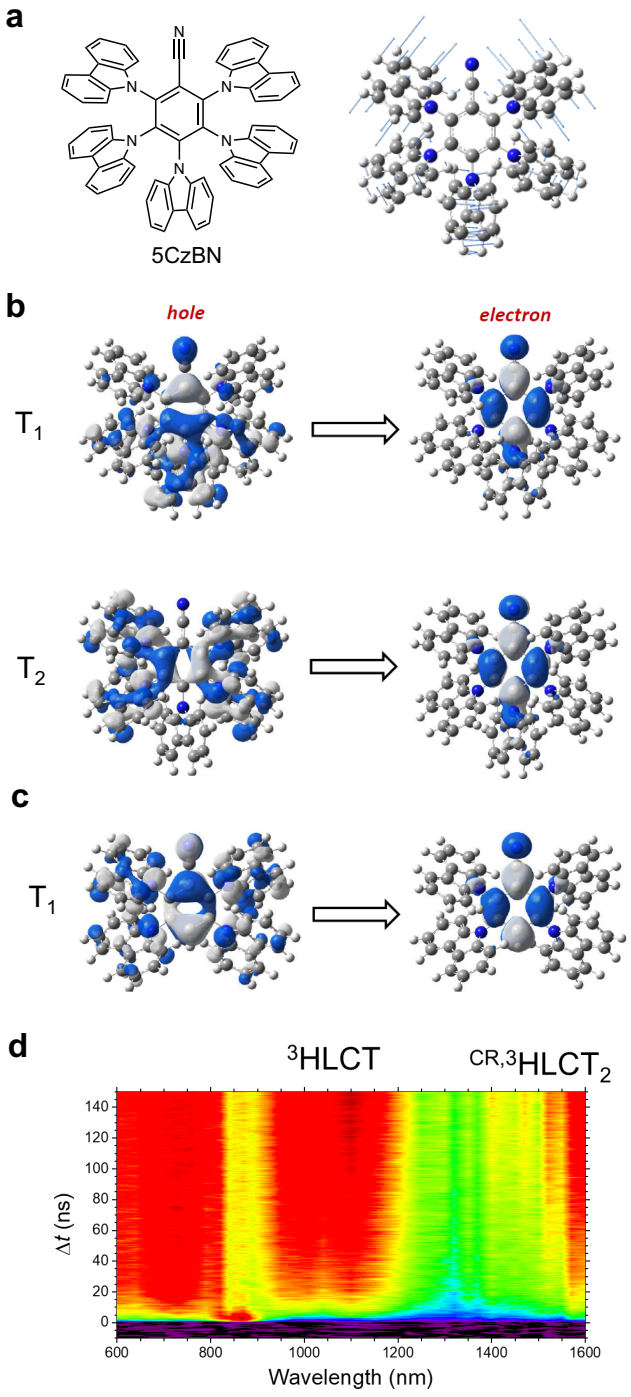

Supplementary Figure 5 | Theoretical description of the excited states of 5CzBN and TAS contour map for 5CzBN in solution. (a) Molecular structure and vibration mode of 5CzBN. (b, c) Molecular orbitals of T_1 and T_2 states in 5CzBN (b) and T_1 state in 4CzBN (c). (d) Contour maps of TAS results for 5CzBN.

Supplementary Figure: Fig. S6

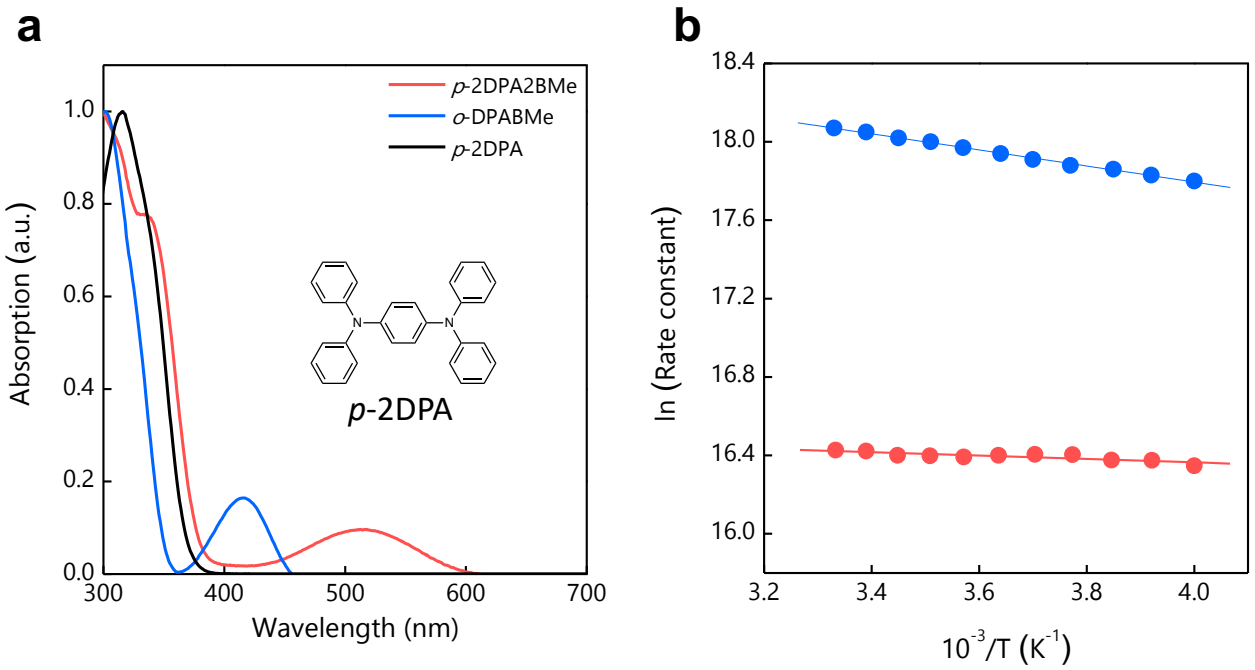

Supplementary Figure 6 | Spin-flip process in *p*-2DPA2BMe. (a) Absorption spectra of *p*-2DPA2BMe (red line), *o*-DPABMe (blue line), and *p*-2DPA (black line), which is one of the possibilities for the absorption band around 350 nm in toluene. Obviously, *p*-2DPA2BMe has no absorption band originating from a partial molecule, *i.e.*, *o*-DPABMe, indicating that, in the ground state, there is no contribution from an electronic structure similar to that of a partial molecular structure. (b) Arrhenius plot of forward ISC: 4CzIPN (blue circle) and *p*-2DPA2BMe (red circle).

Supplementary Figure: Fig. S7

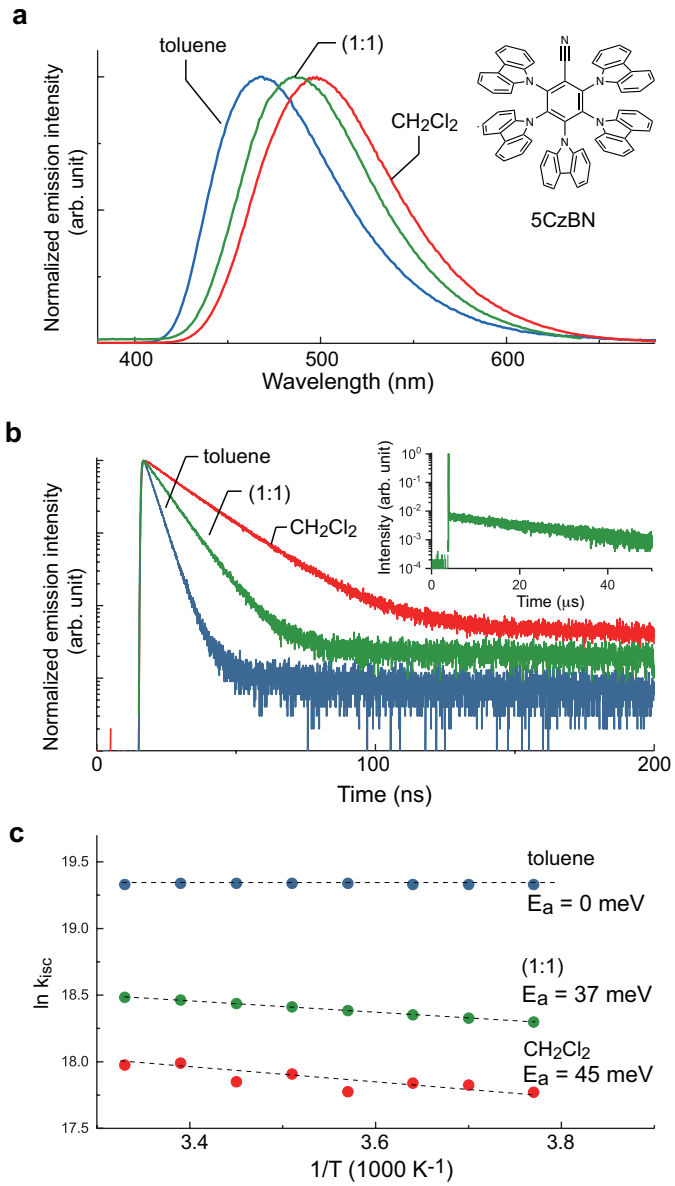

Supplementary Figure 7 | Modulation of intersystem crossing rate by solvation. (a) PL spectra of 5CzBN in toluene (blue), mixed solvent (toluene:dichloromethane = 1:1v/v) (green), and dichloromethane (red) solutions. (b) Transient prompt fluorescence decay curves of 5CzBN in toluene (blue), mixed solvent (toluene:dichloromethane = 1:1v/v) (green), and dichloromethane (red) solutions. Inset: Delayed fluorescence decay curve in mixed solvent (toluene:dichloromethane = 1:1v/v). (c) Arrhenius plot of k_{ISC} in 5CzBN in toluene (blue), mixed solvent (toluene:dichloromethane = 1:1v/v) (green), and dichloromethane (red) solutions. The concentration of the toluene solution was fixed at 10^{-5} mol L^{-1}.

Supplementary Figure: Fig. S8

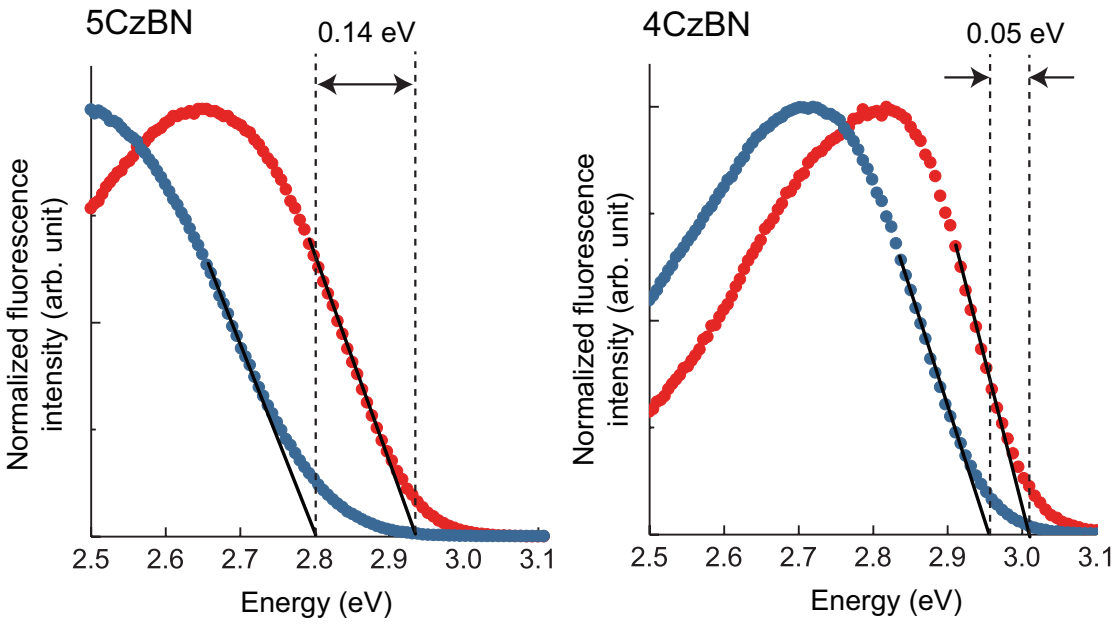

Supplementary Figure 8 | Modulation of excited state energy by solvation. Normalized fluorescence spectrum of 5CzBN (left) and 4CzBN (right) in toluene (red) and CH_2Cl_2 (blue). The solid black lines indicate the threshold of fluorescence spectrum.

Supplementary Figure: Fig. S9

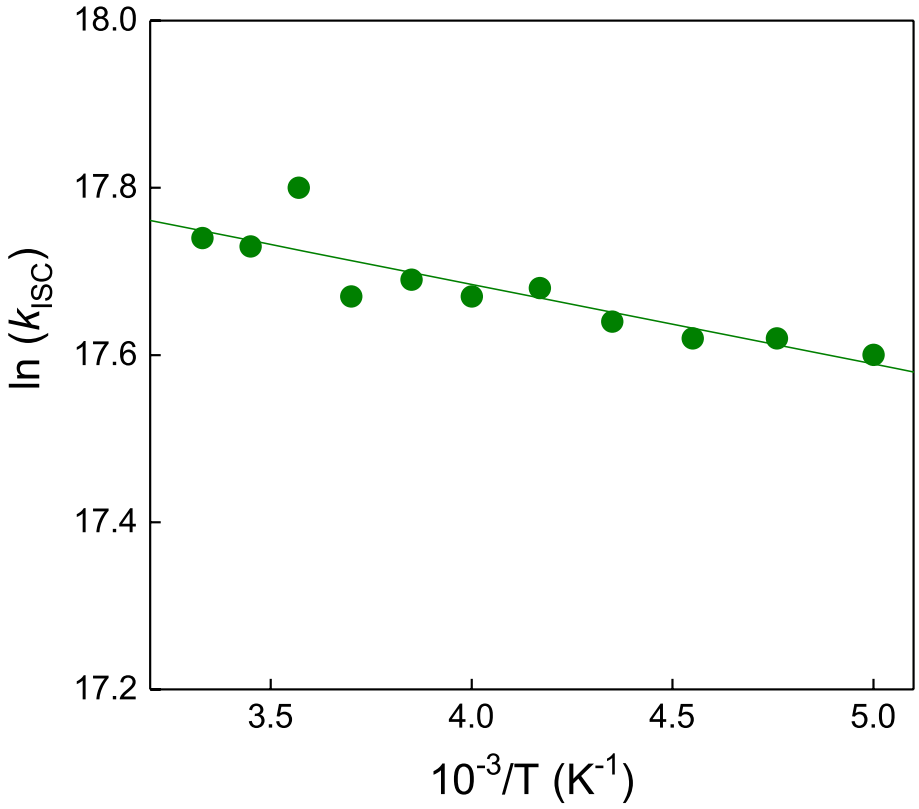

Supplementary Figure 9 | Temperature dependence of spin-flip processes in 4CzIPN in solid-state film. Temperature dependence of the forward ISC rate constants of 4CzIPN in 3,3-di(9H-carbazol-9-yl)biphenyl (mCBP) solid-state host matrix. The solid lines in each figure are fitting results based on arrhenius equation. The concentration of the 4CzIPN was fixed at 5 wt%.

Supplementary Figure: Fig. S10

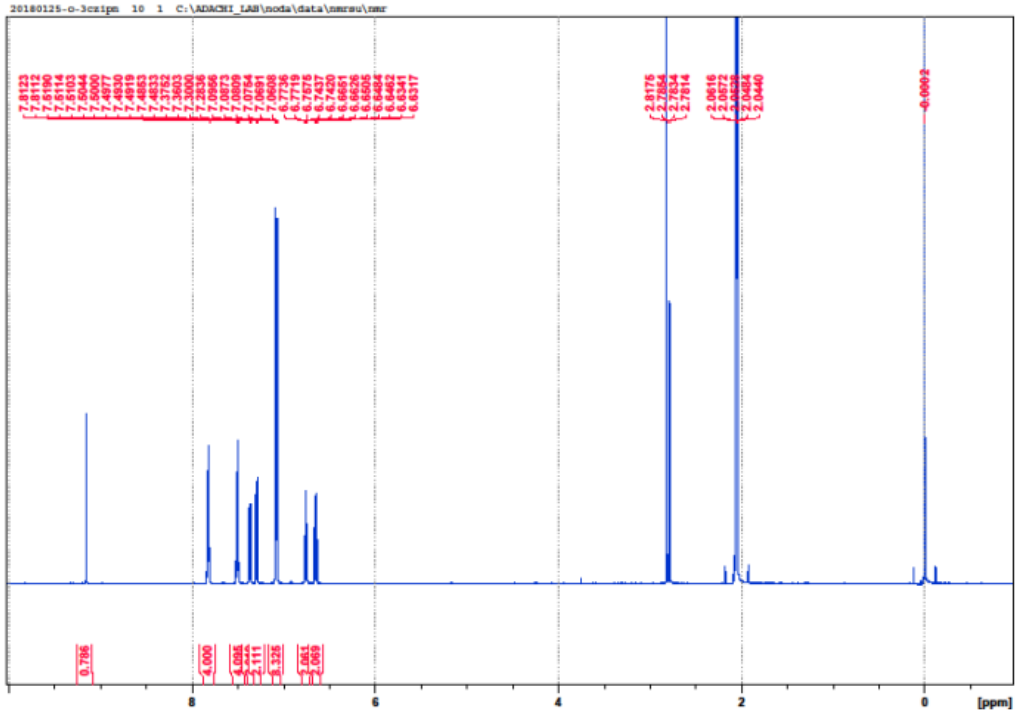

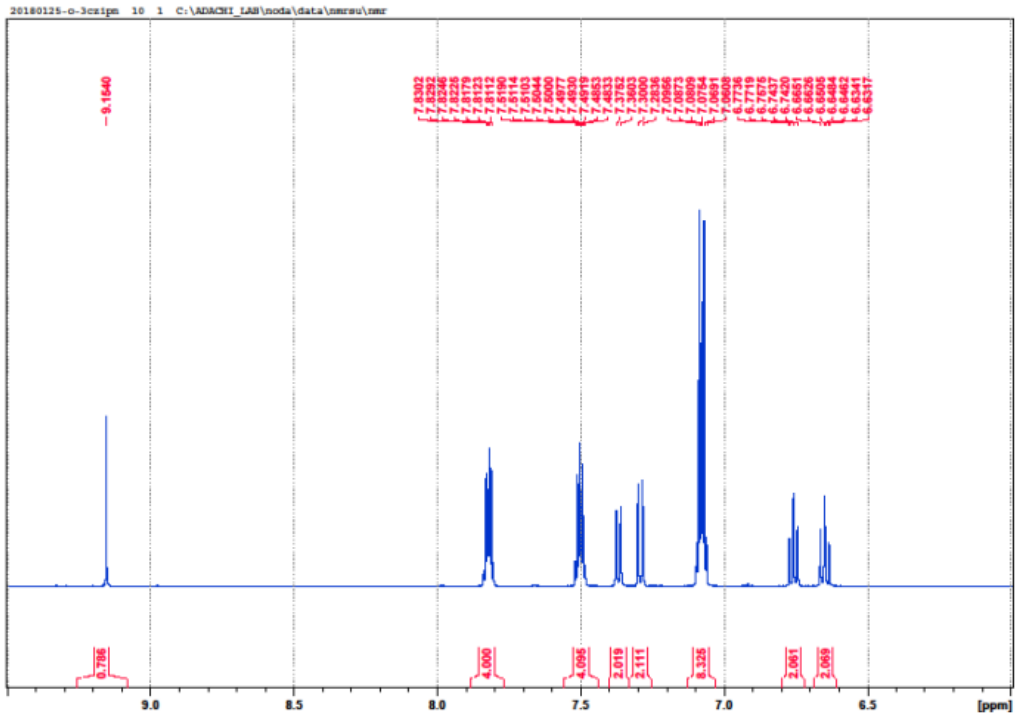

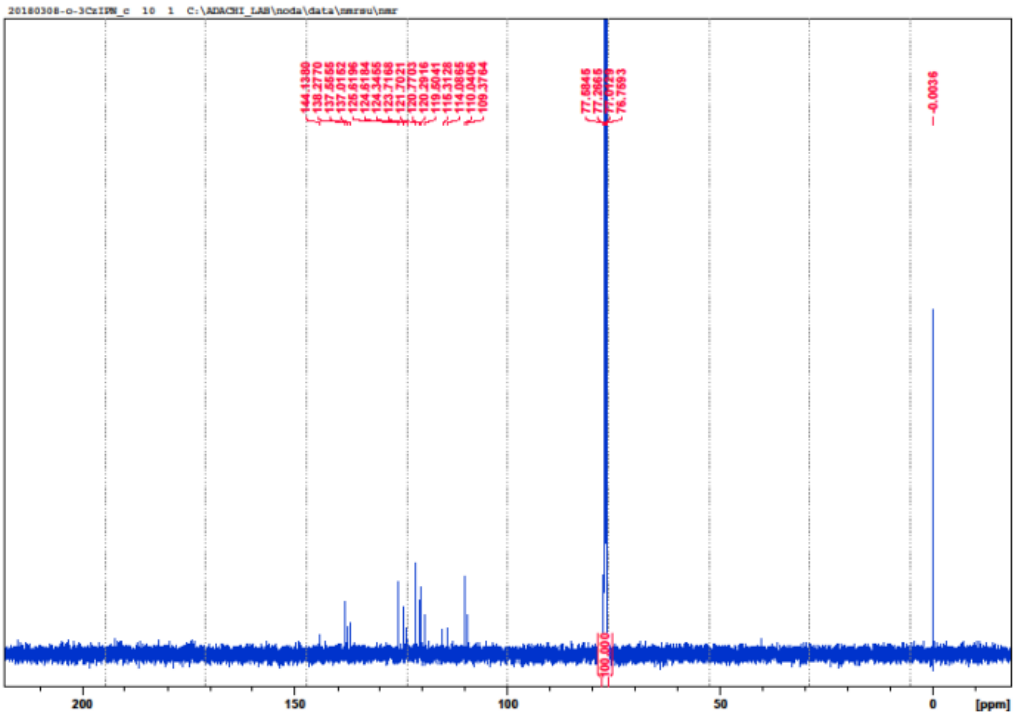

Supplementary Figure 10 | Chemical analysis of o-3CzIPN. ^{1}H and ^{13}C NMR spectra of *o*-3CzIPN.

Supplementary Figure: Fig. S11

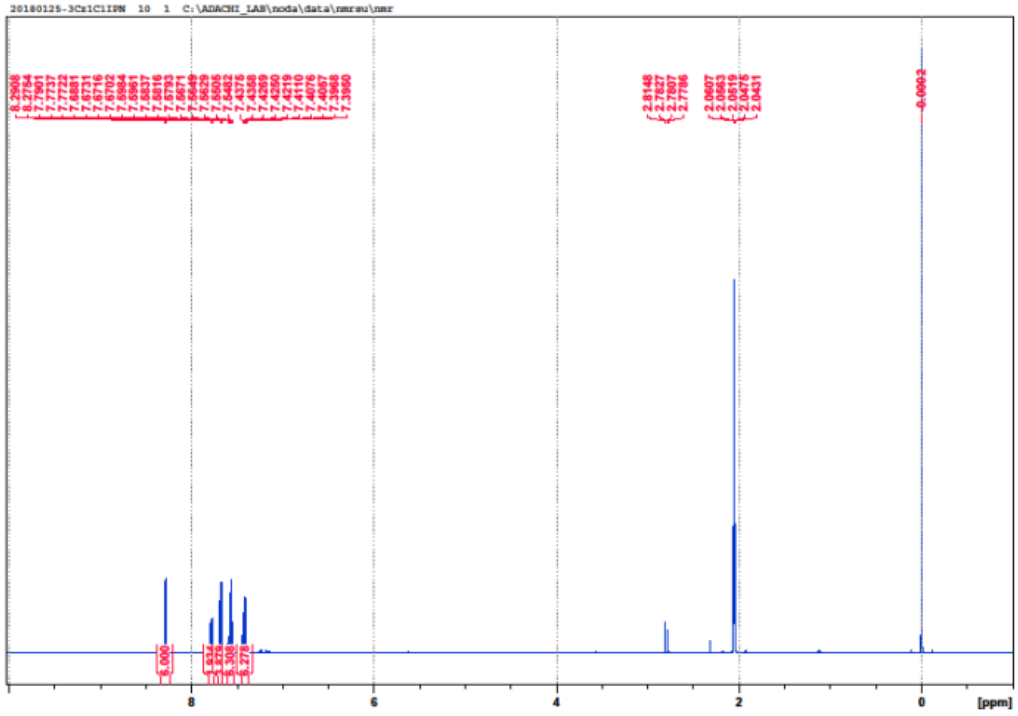

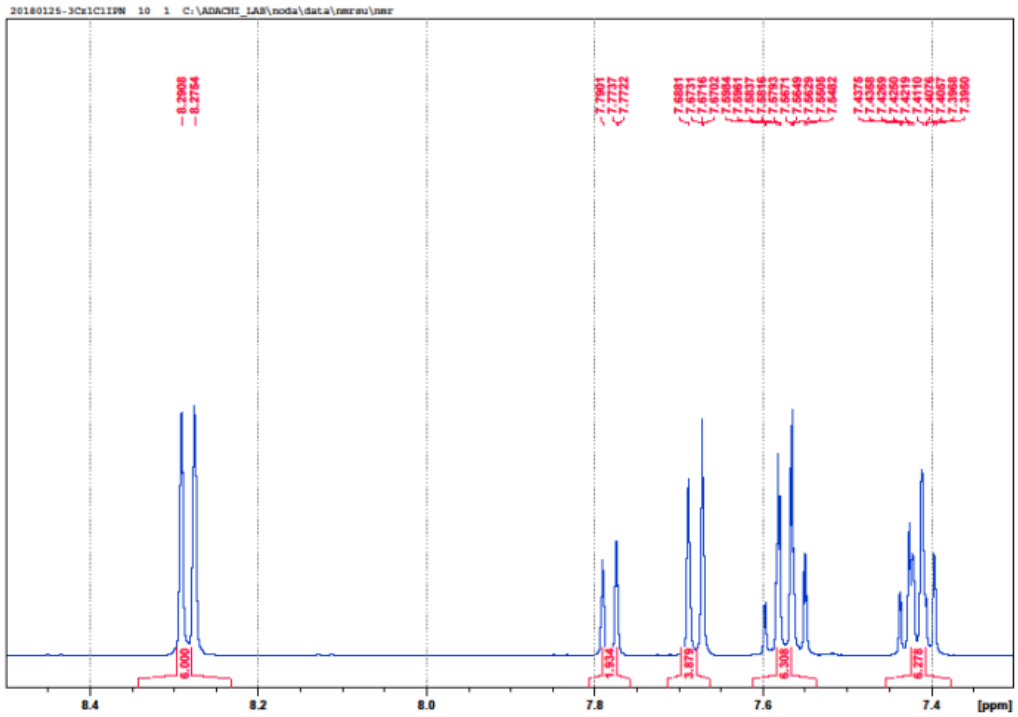

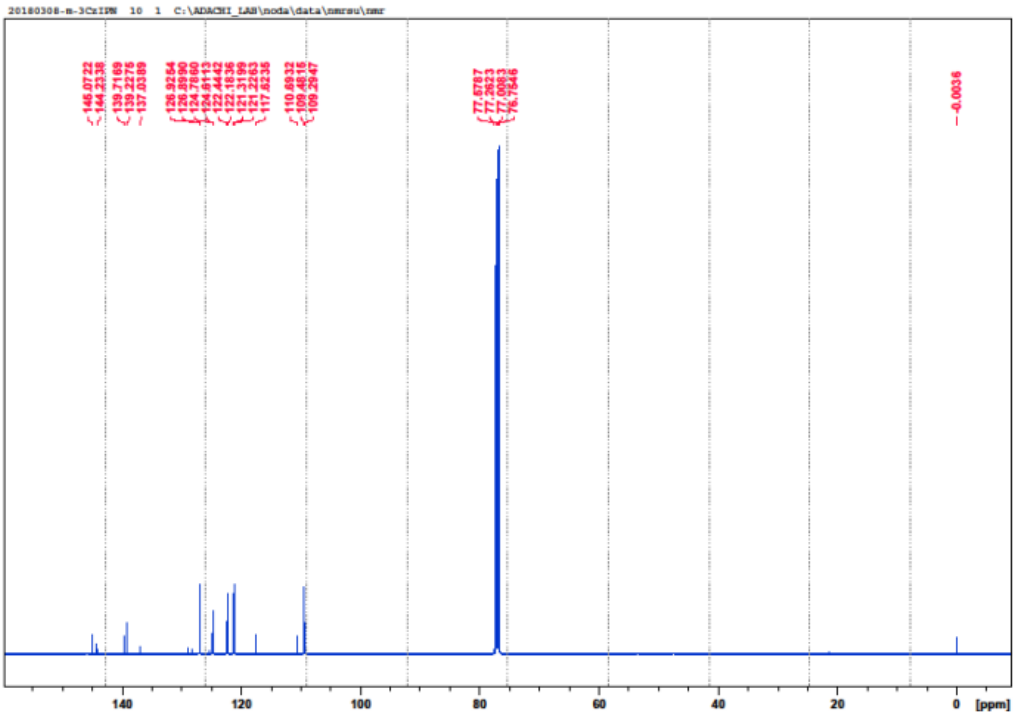

Supplementary Figure 11 | Chemical analysis of *m*-3CzClIPN. ^{1}H and ^{13}C NMR spectra of *m*-3Cz1ClIPN.

Supplementary Figure: Fig. S12

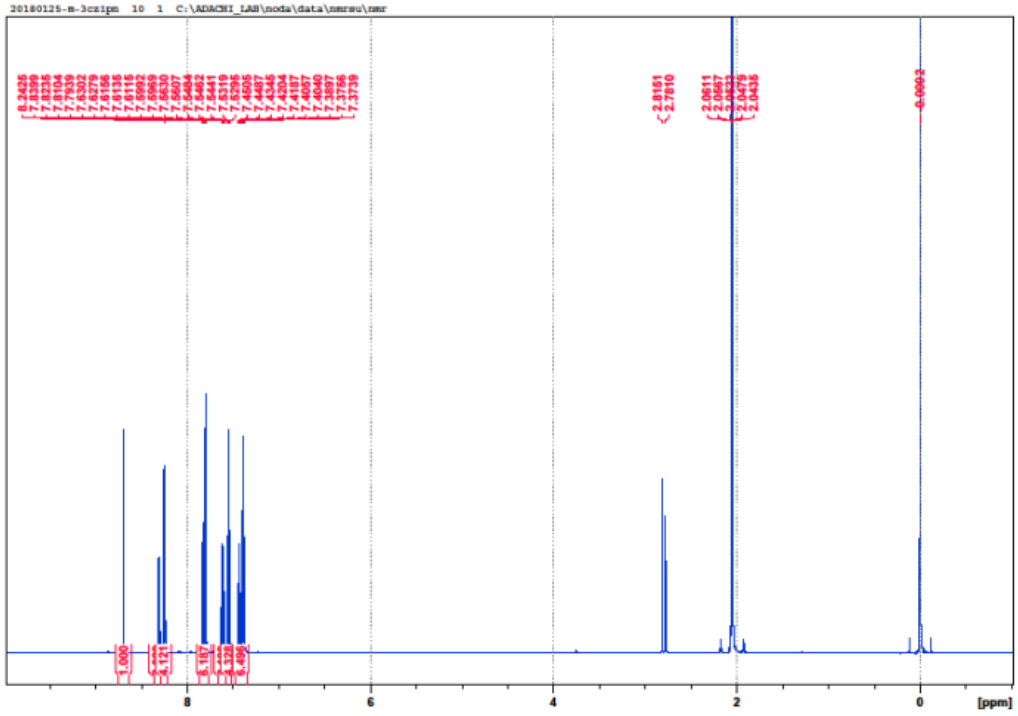

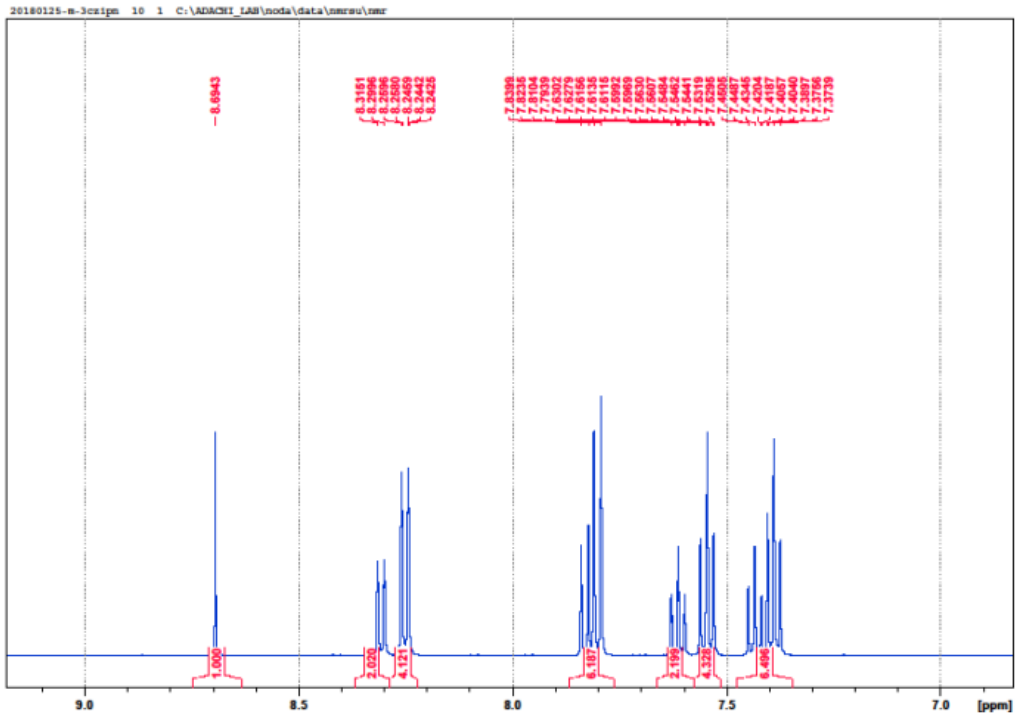

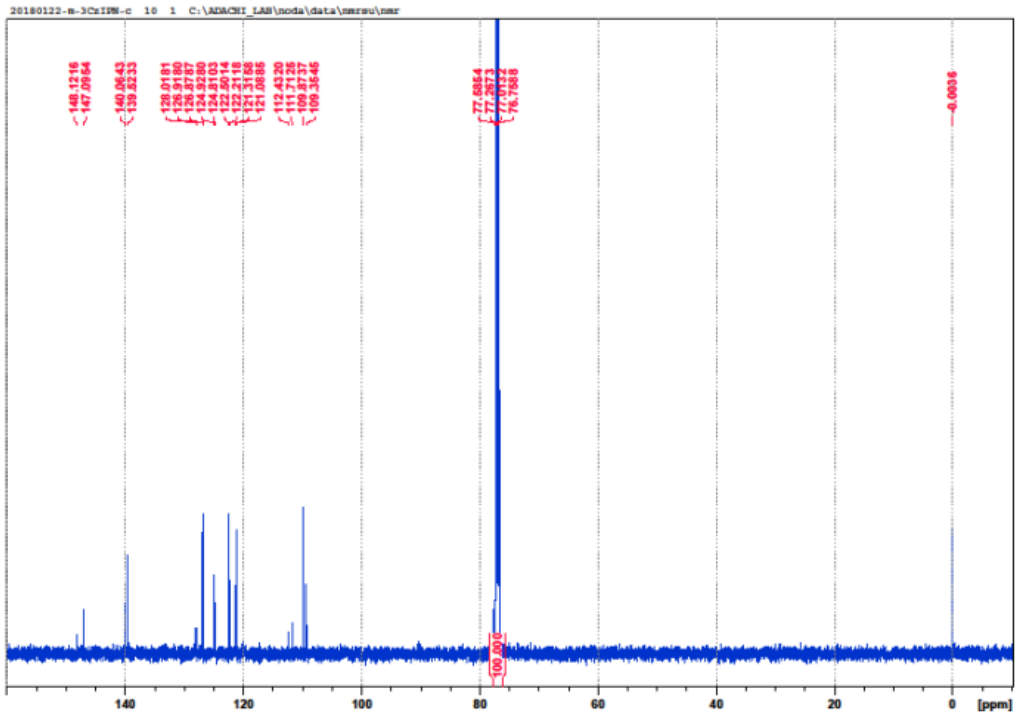

Supplementary Figure 12 | Chemical analysis of *m*-3CzIPN. ^{1}H and ^{13}C NMR spectra of *m*-3CzIPN.

Supplementary Figure: Fig. S13

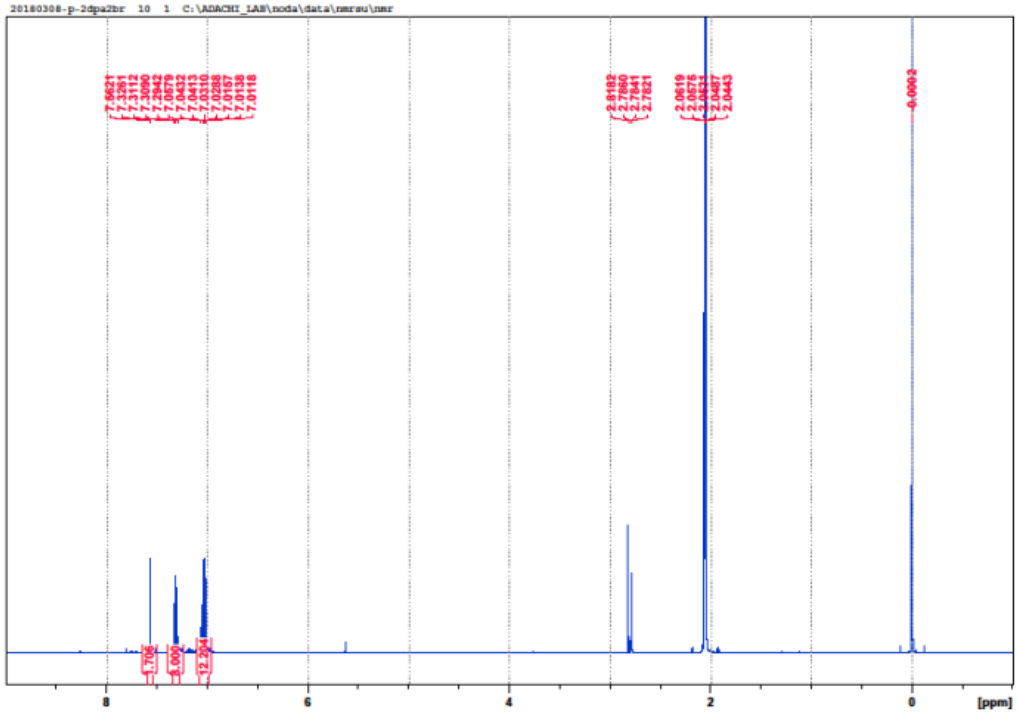

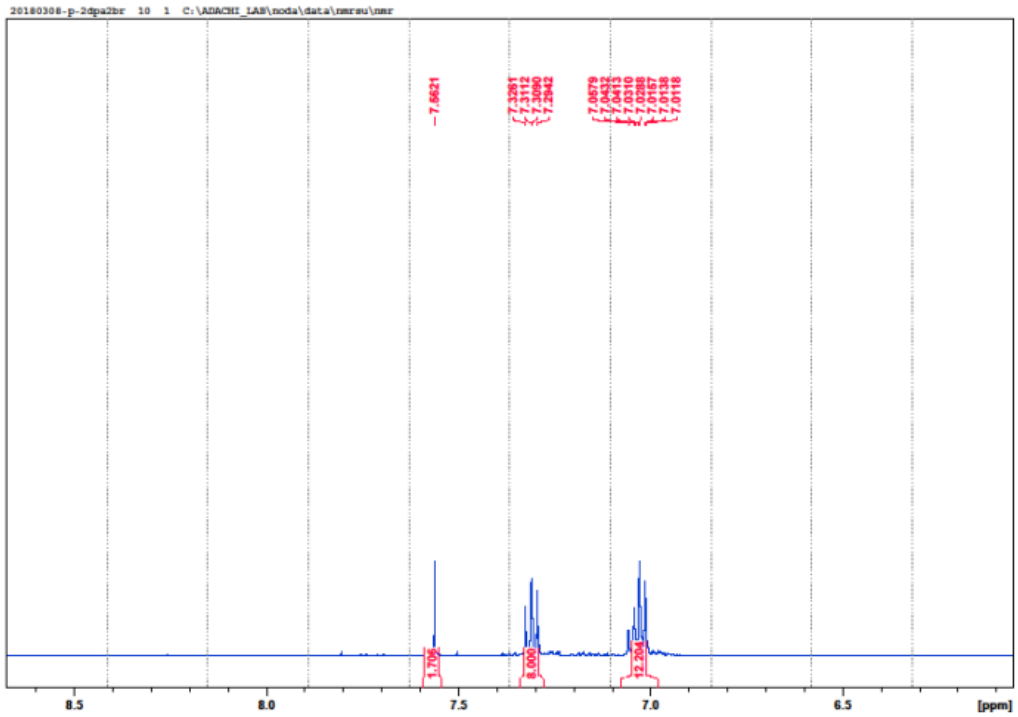

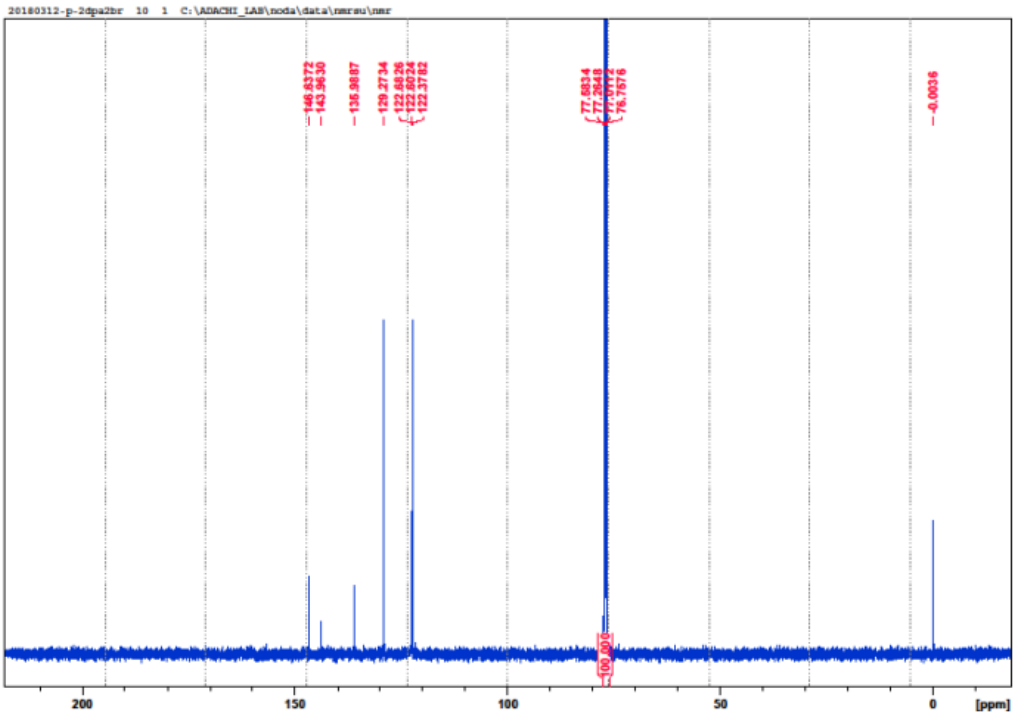

Supplementary Figure 13 | Chemical analysis of *p*-2DPA2Br. ^{1}H and ^{13}C NMR spectra of *p*-2DPA2Br.

Supplementary Figure: Fig. S14

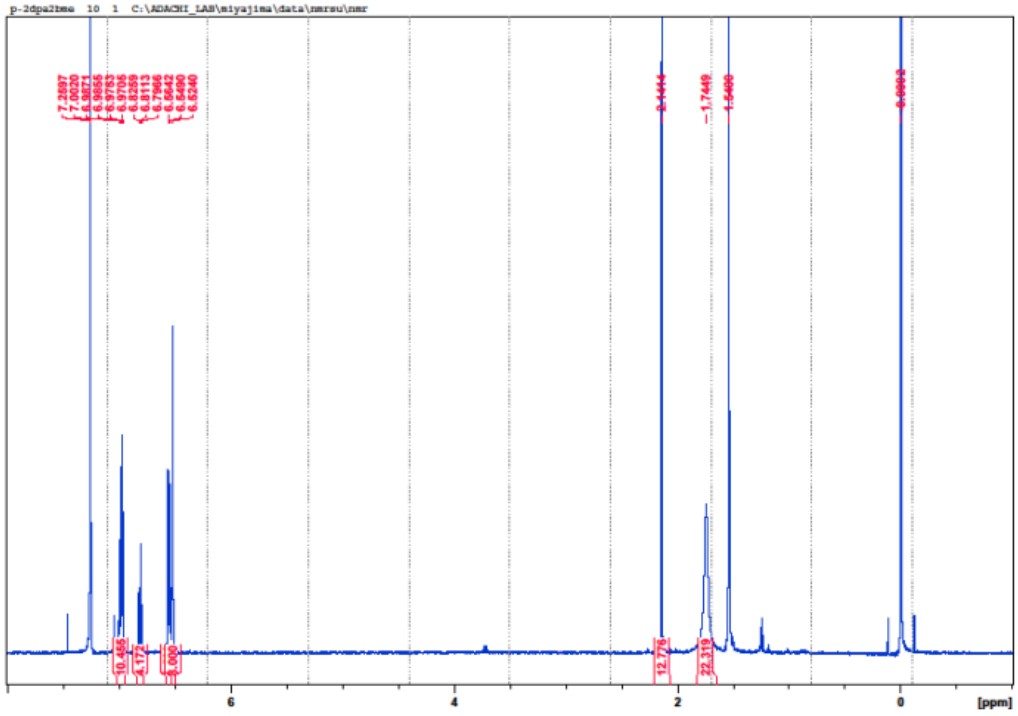

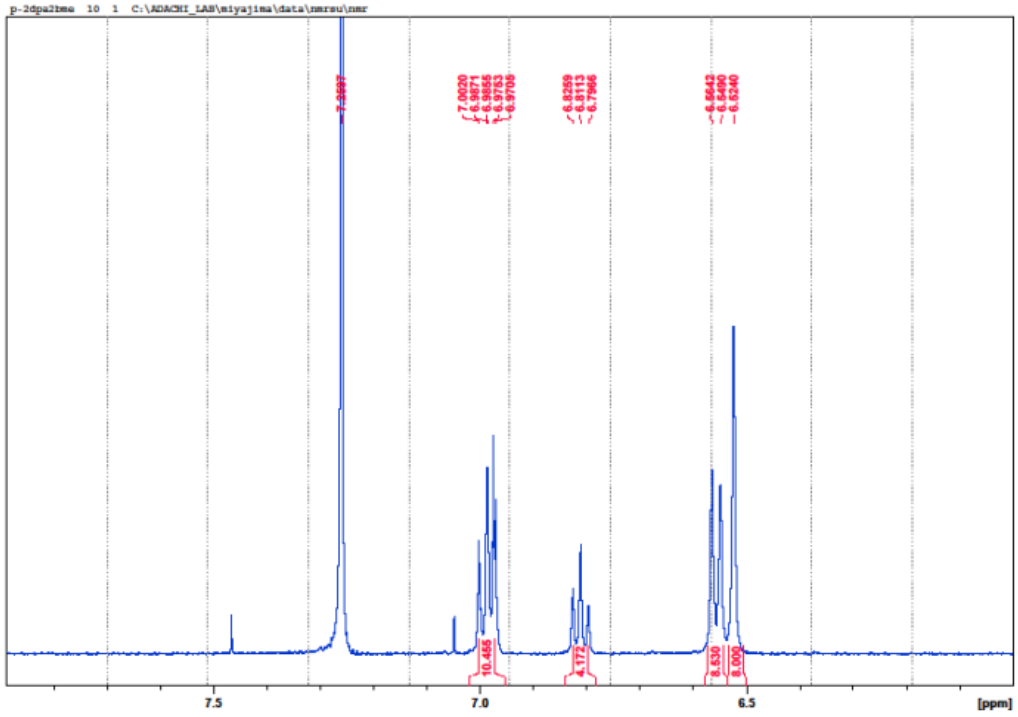

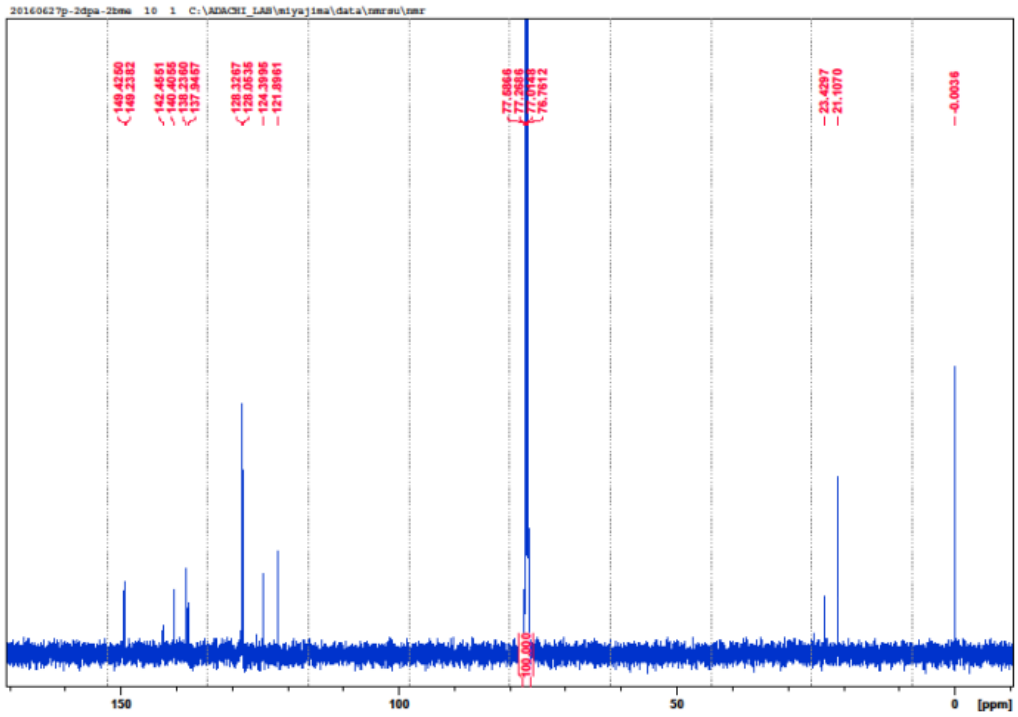

Supplementary Figure 14 | Chemical analysis of *p*-2DPA2BMe. ^{1}H and ^{13}C NMR spectra of *p*-2DPA2BMe.

Supplementary References:

1. Uoyama, H., Goushi, K., Shizu, K., Nomura, H., Adachi, C., Highly efficient organic light-emitting diodes from delayed fluorescence. *Nature,* **492**, 234-238 (2012).

2. Cho, Y. J., Yook, K. S., Lee, J. Y., 20% Cool and warm hybrid white organic light-emitting diode with blue delayed fluorescent emitter both as blue emitter and triplet host. *Sci. Rep.,* **5**, 7859 (2015).

3. Hosokai, T., Matsuzaki, H., Nakanotani, H., Tokumaru, K., Tsutsui, T., Furube, A., Nasu, K., Nomura, H., Yahiro, M., Adachi, C., Evidence and Mechanism of Efficient Thermally Activated Delayed Fluorescence Promoted by Delocalized Excited states. *Sci. Adv.*, **3**, e1603282 (2017).

4. Lee, Y. H., Park, S., Oh, J., Shin, J. W., Jung, J., Yoo, S., Lee, M. H., Rigidity-Induced Delayed Fluorescence by Ortho Donor-Appended Triarylboron Compounds: Record-High Efficiency in Pure Blue Fluorescent Organic Light-Emitting Diodes. *ACS Appl. Mater. Interfaces*, **9**, 24035-24042 (2017).